**archives**
**of thermodynamics**
Vol. **41**(2020), No. 3, 103–123
DOI: 10.24425/ather.2020.134574

# Increasing of efficiency of the cooling duct by modification of its geometry

**KRZYSZTOF KIEDRZYŃSKI***

Department of Thermodynamics, Faculty of Mechanical and Aeronautic Engineering, Rzeszów University of Technology,
Powstańców Warszawy 12, 35-959 Rzeszów, Poland

**Abstract** Increasing of the efficiency of convective cooling of the inner surface of a short duct by changing its geometry was studied by the use of electrochemical limiting current technique (ELDCT). The duct consisted of seven identical, cylindrical segments. The changes of the duct geometry were obtained by mutual displacement of neighbouring segments, towards the radial direction. Mean values of the mass transfer coefficient for each segment and friction losses for the whole channel were measured for Reynolds numbers spanning the range 7700–35300 at the five values of displacement parameter. The results were used for estimation of cooling efficiency. Recommended values of displacement were determined to point the favourable conditions of heat/mass transfer in the duct. The results may be used, e.g. in the design of heat exchangers and channels for cooling of turbine blades and electronic equipment.

**Keywords:** duct electrochemical limiting current technique (ELDCT); heat/mass transfer; efficiency

## Nomenclature

| | | |
|---|---|---|
| $a$ | – | thermal diffusivity, $m^2/s$ |
| $A_k$ | – | surface area of the single cathode, $m^2$ |
| $C$ | – | bulk concentration of reacting ions, $kmol/m^3$ |
| $C_b$ | – | bulk concentration of potassium hexacyanoferrate (III) ions, $kmol/m^3$ |

*Corresponding Author. Email: krzykied@prz.edu.pl

| | | |
|---|---|---|
| $C_s$ | – | concentration of ions at the surface of the cathode, kmol/m$^3$ |
| $D$ | – | diffusivity of ferrocyanide ions in the electrolyte, m$^2$/s |
| $d$ | – | internal diameter of the segments, m |
| $d_h$ | – | hydraulic diameter, m |
| $e$ | – | displacement of neighbouring segments, m |
| $e_w$ | – | displacement ratio $e/d$ |
| $F$ | – | Faraday constant, $96493 \cdot 10^3$ As/kmol |
| $f$ | – | friction factor, $2\Delta p\, d_H/(\rho w^2 L_0)$ |
| $f_{0.0}$ | – | friction factor for the smooth duct ($e_w = 0.0$) |
| $f_{0.265}$ | – | friction factor for the duct ($e_w = 0.265$) |
| $h_D$ | – | mass transfer coefficient for the single segment, m/s |
| $h_{Dm}$ | – | mean value of mass transfercoefficient for the whole duct, m/s |
| $h_M$ | – | mass transfer coefficient, m/s |
| $h_H$ | – | heat transfer coefficient, m/s |
| $I_p$ | – | plateau current, A |
| $I$ | – | current in the circuit, A |
| $j_M$, $j_H$ | – | mean Chilton–Colburn factor for the whole duct for mass and heat transfer, respectively |
| $L_o$ | – | total channel length, m |
| $W$ | – | flow velocity in the duct, m/s |
| $N$ | – | normality of $Na_2S_2O_3 = 0.1$ kmol/m$^3$ |
| $n$ | – | valence charge of reacting ions, $n = 1$ |
| $V$ | – | volume of titrant used, m$^3$ |
| $V_p$ | – | volume of electrolyte sample, m$^3$ |

### Greek symbols

| | | |
|---|---|---|
| $\varepsilon$ | – | electric potential, V |
| $\mu$ | – | dynamic viscosity, kg·m$^{-1}$s$^{-1}$ |
| $\rho$ | – | density of electrolyte, kg/m$^3$ |
| $\eta$ | – | efficiency of the duct |
| $Q$ | – | function, $\Delta\mathrm{Sh}/\Delta f$ |
| $\nu$ | – | kinematic viscosity, m$^2$/s |
| $\Delta p$ | – | pressure drop in the whole duct |

### Dimensionless groups

| | | |
|---|---|---|
| Pr | – | Prandtl number ($= \nu/a$) |
| Re | – | Reynolds number ($= w\, d_h/\nu$) |
| Sc | – | Schmidt number ($= \nu/D$) |
| $\mathrm{St}_M$ | – | Stanton number for mass transfer mean for the whole duct ($= h_M/w$) |
| $\mathrm{St}_H$ | – | Stanton number for heat transfer mean for the whole duct ($= h_D/w$) |
| Sh | – | Sherwood number |
| $\mathrm{Sh}_m$ | – | mean value of Sherwood number for the whole duct ($= h_{Dm} d_h/D$) |
| $\mathrm{Sh}_{0.0}$ | – | mean value of Sherwood number for the smooth duct ($e_w = 0.0$) |
| $\mathrm{Sh}_{0.265}$ | – | mean value of Sherwood number for the duct ($e_w = 0.265$) |

# 1 Introduction

This paper refers to investigation on increasing of cooling efficiency of a short duct under forced flow conditions. The acquired results can be used in the design of heat exchangers and channels for cooling of turbine blades and electronic equipment. The duct consists of seven cylindrical segments, made of nickel, and distribution of mass transfer coefficient $h_D$ was measured for three different configurations as shown in Fig. 1.

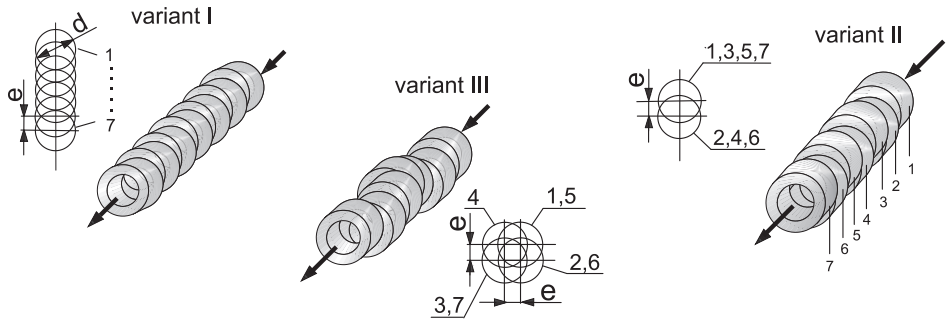


Figure 1: Configurations of the duct, Bieniasz [1].

The configurations were attained by mutual displacement of neighbouring segments in three different arrays (Fig. 1). The effects of turbulence caused by the displacements were studied by the use of electrochemical limiting current technique. For one value of displacement $e$, maintaining the surface area of heat/mass transfer for each configuration to be equal, the mean values of the Chilton–Colburn factor $j_M$ for mass transfer for the whole duct were measured for the Reynolds number from the range 7600–44200. The factor $j_M$ was calculated on the basis of the well known Chilton–Colburn analogy, according to which

$$j_M = \mathrm{St}_M \, \mathrm{Sc}^{2/3} \, . \tag{1}$$

Mean values of $j_M$ coefficient were stated for three configurations and presented in Fig. 2.

The variant III of the duct was made available to be investigated in this work. The configuration was chosen for its highest values of $j_M$ factor from

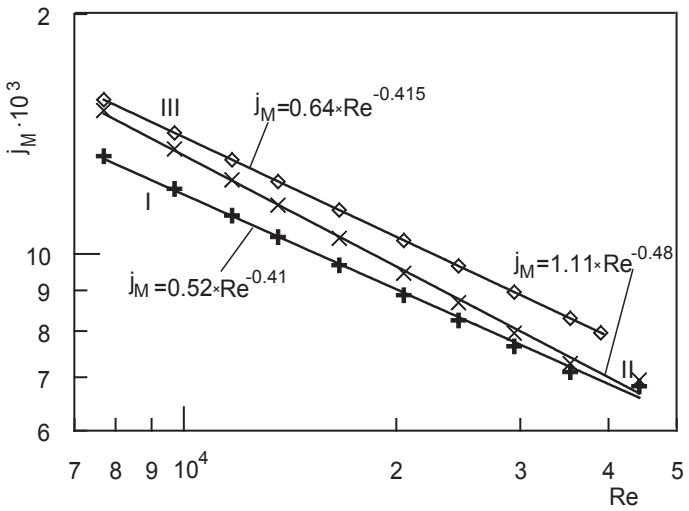


Figure 2: Mean value of $j_M$ and appropriate correlation factor for the whole duct, Bieniasz [1].

among the three ones in the pointed range of Reynolds numbers. The aim of the work was to determine the values of displacement $e$ at which the higher efficiency of convective cooling could be reached in the duct.

Some previous works related to the subject can be found. Sethumadhavan *et al.* [2] using the thermal technique, studied the efficiency of a 25 mm I.D. copper tube where the various effects of turbulization were attained by tightly fitted helical-wire-coil inserts of varying pitch, helix angle and wire diameter. The efficiency was determined on the basis of maximization of heat transfer and minimization of pumping power.

Liao Q. *et al.* [3] investigated the heat transfer and friction characteristics for water, ethylene glycol and ISO VG46 turbine oil flowing inside four tubes with three-dimensional internal extended surfaces and copper continuous or segmented twisted-tape inserts. The experimental results indicated 2.8-fold increase of average Stanton number in the laminar flow and a 4.5-fold increase in transitional and turbulent flows as compared to smooth tubes. Simultaneously, the friction factor was increased by 1.7-fold in laminar flow and 4-fold in transitional and turbulent flow. The thermal performance ratio was the highest for the continuous twisted-tape insert case.

Chang S.W. *et al.* [4], using the infrared radiometer technique, determined the end-wall heat transfer and pressure drop characteristics in a rectangular channel with a channel aspect ratio of 4 and the staggered arrange-

ment of circular pin-fins with four clearances ($C$) between pin-tips and the measured end-wall of 0, 1/4, 1/2, and 3/4 pin-diameter ($d$). The four cases were examined comparatively at Reynolds numbers between 10.000 and 30.000. The thermal performance factor was the highest at $C/d = 1/4$ in studied range of Reynolds numbers which was caused by comparatively low pressure drop coefficient in that case.

Andrzejczyk *et al.* [17] investigated individual heat exchanger constructions with plain double tube, turbulized double tube , plain U-bend and U-bend with turbulator. Tests were made for the water–water system for a constant temperature of 9 °C and 50 °C. The heat exchangers were made from copper tubes with external diameter of 10 mm and 18 mm respectively and wall thickness of 1 mm. The helicoidal vortex generator was made from brass wire with a diameter of 2.4 mm, coil diameter of 13 mm and pitch of 11 mm. Reynolds numbers spanning the range 800–9000. Wire coil turbulator increased the heat transfer coefficient (HTC) over 100% and pressure drop up by 100%.The modified construction achieved a similar efficiency.

## 2 Experimental technique

There exists similarity between heat transfer forced by temperature difference and diffusion mass transfer caused by the difference of its concentration. In the work the well-known electrochemical limiting diffusion current technique (ELDCT) was used.

It allowed to determine mass transfer coefficient $h_M$ on the basis which heat transfer coefficient $h_H$ can be calculated by using a well known Chilton-Colburn analogy:

$$j_M = \mathrm{St}_M \mathrm{Sc}^{2/3}, \tag{2}$$

$$j_H = \mathrm{St}_H \mathrm{Pr}^{2/3}, \tag{3}$$

$$j_M = j_H \,. \tag{4}$$

In the electrochemical technique magnitude of mass (ions of potassium hexacyanoferrate (III)), transferred towards the cathode during the diffusion controlled ($C_s = 0$), is determined by the value of the current measured in the external part of the electric circuit, presented in Fig. 3. The inner surface of the researched duct was the nickel cathode. The anode was made of the same material.

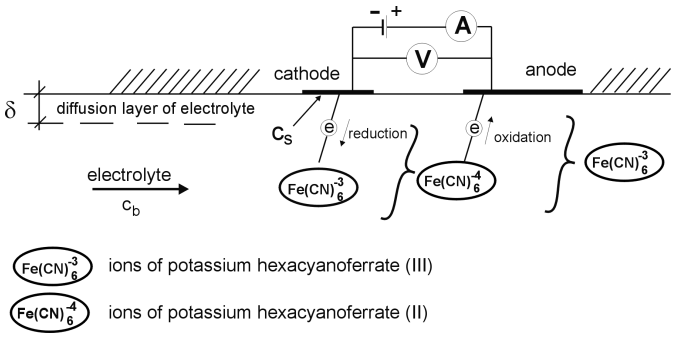


Figure 3: Electrode process performance.

The state of diffusion controlled has place when the changes of electric tension between the electrodes do not influence on the value of the current flowing in the circuit (Fig. 4). The value $I_p$ and the bulk concentration of potassium hexacyanoferrate (III) are used to calculate the value of mass transfer coefficient from the relation

$$h_D = I_p/(nFA_kC_b). \tag{5}$$

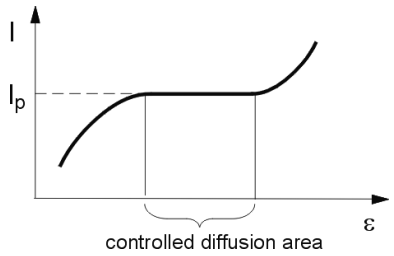


Figure 4: Polarization curve.

In the literature lots of papers can be found where the electrochemical limiting diffusion current technique is especially useful to determine heat/mass transfer e.g. in minichannels [9–11] or in mini heat exchangers [12]. More details on the ELDCT technique are given in [5].

## 3 Apparatus

The measurements were performed on the rig presented in Fig. 5. To make measurements more accurate and convenient data acquisition card, intelli-

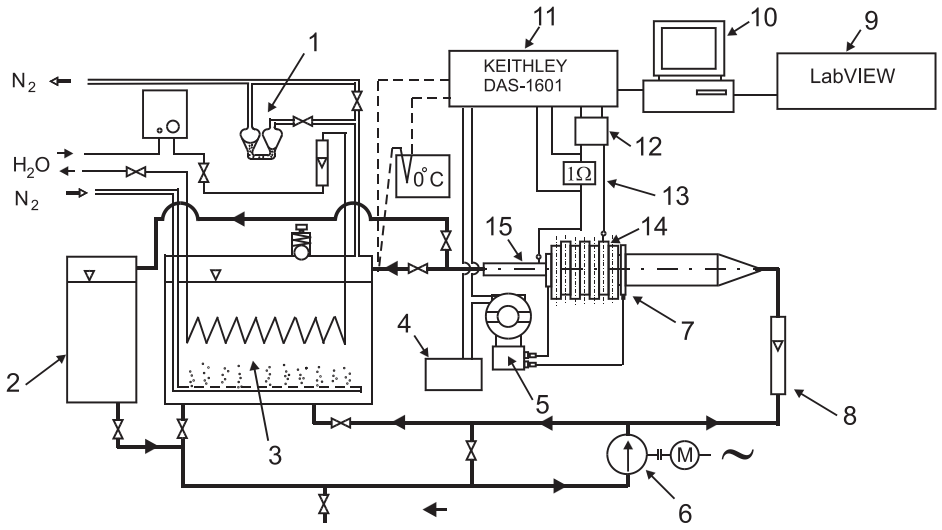


Figure 5: Scheme of the rig: 1 – visual control of $N_2$ flux, 2 – tank with electrolyte for activation, 3 – main tank with cooling coil, 4 – DC Power Supply, 5 – differential pressure transmitter LD 301 SMART, 6 – pump, 7 – test section, 8 – rotameter, 9 – software, 10 – PC-computer, 11 – data acquisition card, 12 – current amplifier, 13 – standard resistor, 14 – cathode, 15 – anode.

gent differential pressure transmitter and the proper software were used in the rig.

The test section was shown in Fig. 6.

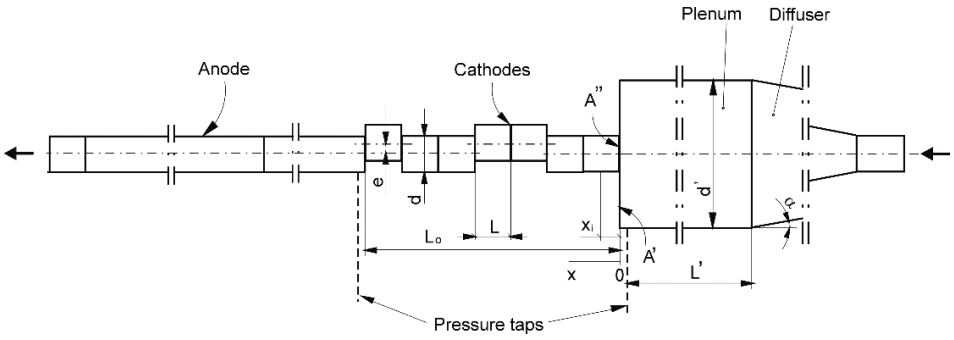


Figure 6: Test section.

Potassium hexacyanoferrate (II) and (III) of equimolar quantities, were dissociated in aqueous solution of 1 M NaOH. The electrodes were made of

nickel where the cathode was the inner surface of the duct investigated. The segments of the duct were fixed in rectangular PCV plates what ensures the segments to be displaced comfortably. Between the neighbouring plates thin sheets of electrolyte resistant rubber were placed. All elements were squeezed tightly in the special housing to make the duct leak-proof. The length of the duct, after squeezing, was 142 mm. The flow of the electrolyte through the channel was forced by the presence of the pump. Undesirable oxygen in the electrolyte was removed by $N_2$. The temperature of the electrolyte was kept at the constant value of 25°C at which its basic parameters were: $D = 6.71 \times 10^{-10}$ m$^2$s$^{-1}$, $\mu = 1.11 \times 10^{-3}$ kg m$^{-1}$s$^{-1}$, $\rho = 1040$ kg m$^{-3}$. Special attention was paid for preparing the working surfaces of the segments. Finally, they were polished with the diamond paste 1/0 as a type of polishing compound made from finely ground or powdered diamond particles and some kind of liquid, which was water based.

## 4 Results of measurements and discussion

On the base of polarization curves the limiting current $I_p$ for every segments of the duct and pressure loss for all the duct were determined for 9 values of Reynolds number at the parameter $e = 0.0$, 1.5, 3.0, 4.5, 6.0 mm with relative displacement $e_w = 0.0$, 0.088, 0.177, 0.266, 0.354, respectively. The ferrocyanide ion concentration was measured by iodometric titration according to the formula

$$C_b = 10^{-3} V N / V_p \,, \tag{6}$$

where $V$ – volume of titrant used, m$^3$, $V_p$ – volume of electrolyte sample, m$^3$, N – normality of $Na_2S_2O_3 = 0.1$ kmol/m$^3$.

For each value of displacement $e_w$ the distribution of mean value of mass transfer coefficient $h_D$ for particular cathodes vs segment position at the parameter Re was made (Fig. 7).

The assumed $Q$ function

$$Q = \Delta \mathrm{Sh} / \Delta f \tag{7}$$

determines the change of heat/mass transfer related to the change of energy needed to overcome the flow resistance of working medium caused by the change of displacement $e$. $\Delta$Sh and $\Delta f$ were attained as shown in Figs. 8 and 9. The following values of $\Delta$Sh and $\Delta f$ were referred to the Sh and $f$ values of the smooth duct ($e_w = 0$), respectively.

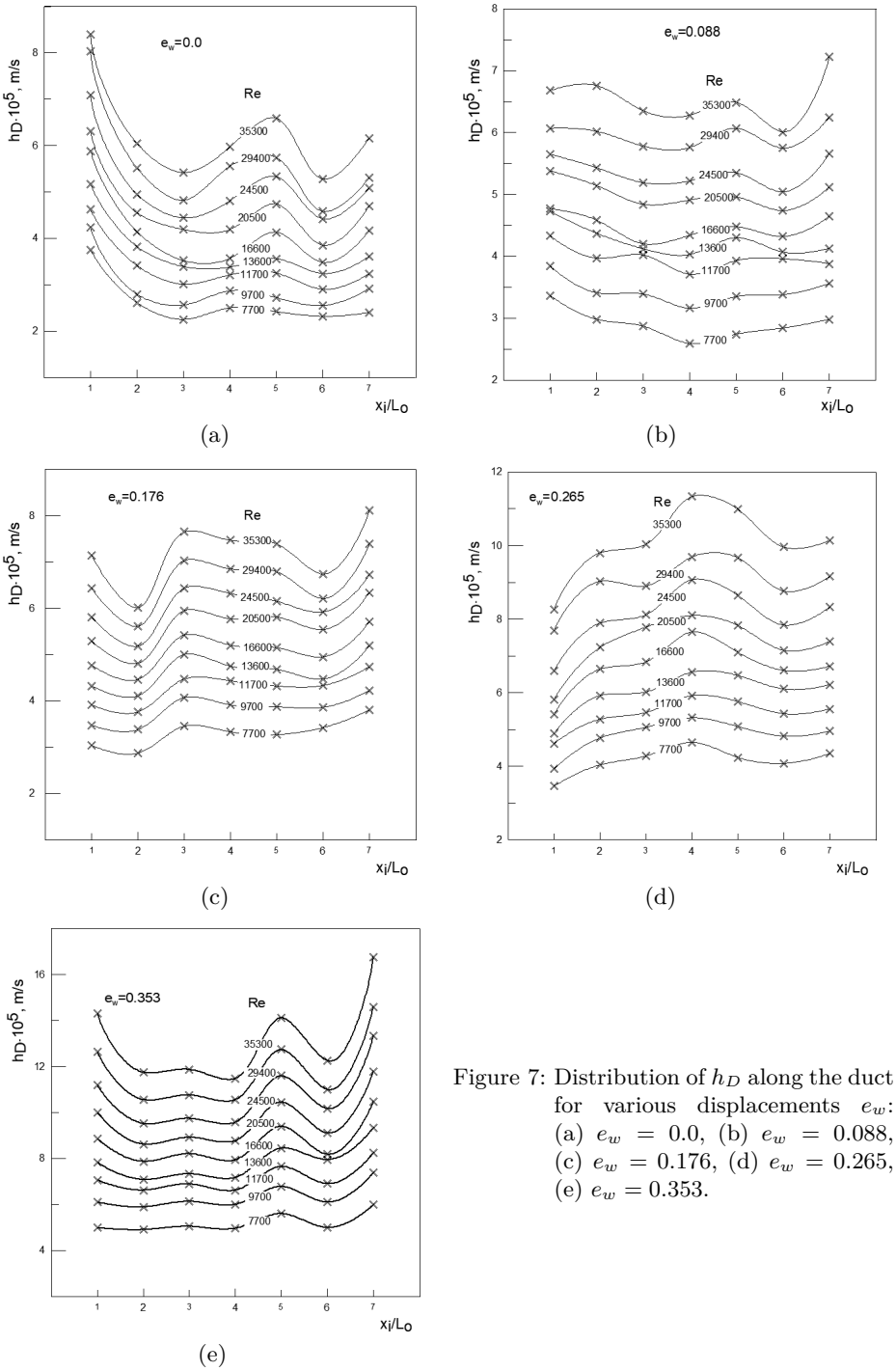


Figure 7: Distribution of $h_D$ along the duct for various displacements $e_w$: (a) $e_w = 0.0$, (b) $e_w = 0.088$, (c) $e_w = 0.176$, (d) $e_w = 0.265$, (e) $e_w = 0.353$.

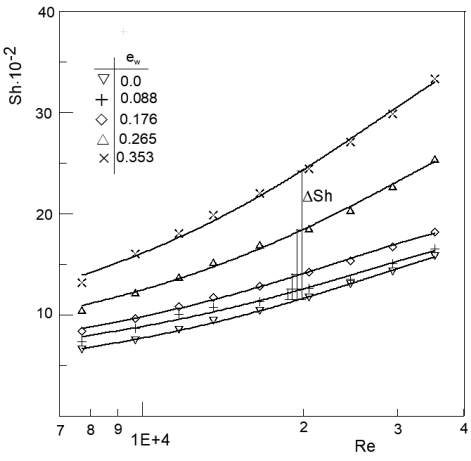


Figure 8: Sherwood number vs Re for the used displacements.

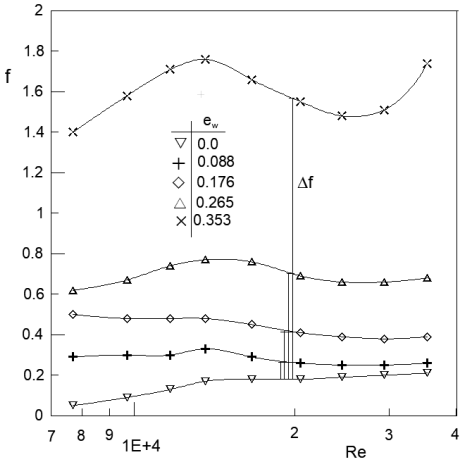


Figure 9: Friction losses factor vs Re for the used displacements.

The mean values of Sh for the whole duct were calculated from

$$\mathrm{Sh} = \frac{h_{Dm}\, d_h}{D}\,, \tag{8}$$

where the hydraulic diameter $d_h$ was assumed as equal $d$.

The Fanning friction factor $f$ for the studied duct was given by

$$f = \frac{\Delta p}{\dfrac{\rho W^2}{2}\dfrac{L_o}{d_h}}\,. \tag{9}$$

On the base of $\Delta\mathrm{Sh}$ and $\Delta f$ values determined in Fig. 8 and 9, the distribution of $Q$ was presented in Fig. 10 and its values were given in Tab. 1.

The growing value of displacement ratio $e_w$ was followed by the growing value of mass transfer coefficient Sh (Fig. 8) and growing value of friction losses $f$ (Fig. 9). The neighbourhood of $e_w = 0.265$ was pointed to be interested for the highest value of $Q$ function in the whole range of displacements.

It was assumed that the measure of efficiency of the duct was the function:

$$E = \left(\frac{\mathrm{Sh}}{f}\right) \Big/ \left(\frac{\mathrm{Sh}_0}{f_0}\right), \tag{10}$$

where: $\mathrm{Sh}_0$, $f_0$ – parameters of the smooth duct ($e_w = 0.0$).

The distribution of $E$ function was shown in Fig. 11 on the basis of Tab.2.

Table 1: Values of $Q$ distribution with the $Q_{\max}$ marked in the frame.

| Re | $e_w$ | | | |
|---|---|---|---|---|
| | 0.089 | 0.177 | 0.265 | 0.354 |
| 7700 | 330 | 416 | 727 | 515 |
| 9700 | 626 | 601 | 874 | 608 |
| 11700 | 888 | 681 | 895 | 632 |
| 13600 | 900 | 798 | 1021 | 694 |
| 16600 | 859 | 984 | 1187 | 823 |
| 20500 | 1220 | 1203 | 1415 | 981 |
| 24500 | 801 | 1209 | 1632 | 1149 |
| 29400 | 1483 | 1375 | 1916 | 1255 |
| 35300 | 1392 | 1387 | 2158 | 1208 |

Table 2: Values of Sh and $f$.

| Sh | | | | | | | | | |
|---|---|---|---|---|---|---|---|---|---|
| $e_w$ | Re | | | | | | | | |
| | 7700 | 9700 | 11700 | 13600 | 16600 | 20500 | 24500 | 29400 | 35300 |
| 0.0 | 658 | 745 | 852 | 944 | 1042 | 1172 | 1303 | 1426 | 1581 |
| 0.089 | 734 | 868 | 1002 | 1075 | 1129 | 1264 | 1353 | 1502 | 1650 |
| 0.177 | 837 | 967 | 1081 | 1175 | 1287 | 1426 | 1535 | 1671 | 1824 |
| 0.265 | 1050 | 1224 | 1371 | 1521 | 1694 | 1849 | 2037 | 2269 | 2543 |
| 0.354 | 1315 | 1601 | 1803 | 1989 | 2198 | 2441 | 2710 | 2988 | 3338 |
| $f$ | | | | | | | | | |
| $e_w$ | Re | | | | | | | | |
| | 7700 | 9700 | 11700 | 13600 | 16600 | 20500 | 24500 | 29400 | 35300 |
| 0.0 | 0.05 | 0.09 | 0.12 | 0.16 | 0.17 | 0.17 | 0.18 | 0.19 | 0.20 |
| 0.089 | 0.28 | 0.29 | 0.29 | 0.31 | 0.27 | 0.25 | 0.24 | 0.24 | 0.25 |
| 0.177 | 0.48 | 0.46 | 0.46 | 0.45 | 0.42 | 0.38 | 0.37 | 0.36 | 0.37 |
| 0.265 | 0.59 | 0.64 | 0.70 | 0.73 | 0.72 | 0.65 | 0.63 | 0.63 | 0.64 |
| 0.354 | 1.32 | 1.50 | 1.62 | 1.67 | 1.58 | 1.47 | 1.40 | 1.43 | 1.65 |

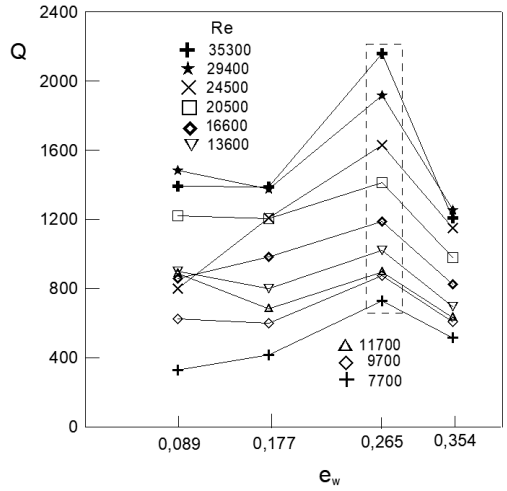


Figure 10: Distribution of $Q$ function.

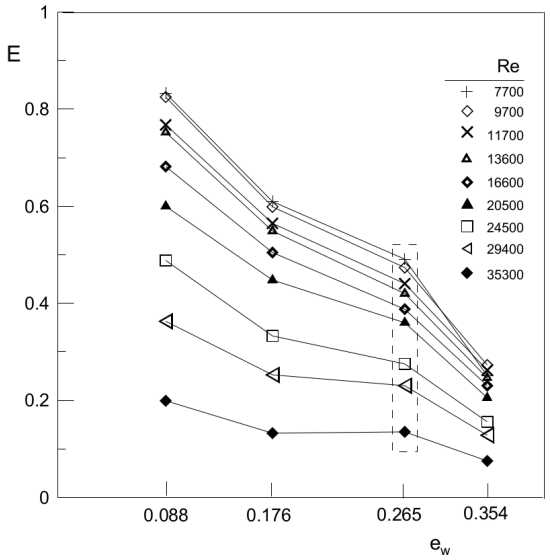


Figure 11: Distribution of $E$ function.

## 5 Measurement uncertainties analysis

**The uncertainty of heat/mass transfer analogy.** The measurement results include uncertainties related to the experimental method accuracy

and mass/heat transfer analogy. Wilk [7] concluded that research results of the flow through a circular channel, by the use of electrolytic technique and theoretical analysis or thermal tests, were similar to each another for the Reynolds number from the range 6000–20000. The author attempted to estimate the uncertainty of the heat/mass transfer analogy basing on the research results of the industrial process of heating of the batch in metallurgical furnace [8], where the comparison of results, obtained by means of heat, electrolytic, and naphthalene test, was carried out. Finally, the author estimated the uncertainty of heat/mass transfer analogy on 10%–25% in the investigated range of Re.

**Measurement accuracy.** The main goal was to determine the uncertainties of $Q$ function values which were calculated according to the general formula:

$$\frac{\Delta Q}{Q} = \sqrt{\frac{\sum_{i=1}^{n} \left( \frac{\partial Q}{\partial X_i} \Delta X_i \right)^2}{Q^2}}, \tag{11}$$

where $\Delta X_i$ – the mean uncertainties of the partial measurements.

The most pronounced uncertainty of the mass transfer coefficient measurement is in the neighbourhood of displacement where the function $Q = Q_{\max}$ in the investigated range of Re. For $e_w = 0.265$, the geometry parameters of the analysed duct with their uncertainties are shown in Tab. 3.

Table 3: Geometry parameters of the duct for $e_w = 0.265$.

| Geometry of the duct | | | |
|---|---|---|---|
| $A_{Ki} \cdot 10^4$ [m$^2$], $i = 1 \ldots 7$ | $\Delta A_{Ki} \cdot 10^7$ [m$^2$] | $(d = d_h) \cdot 10^3$ [m] | $(\Delta d = \Delta d_h) \cdot 10^5$ [m] |
| 11.373 | 6.73 | 16.88 | 1 |
| 12.131 | | 16.95 | |
| 12.09 | | 16.93 | |
| 12.06 | | 16.83 | |
| 12.115 | | 16.98 | |
| 12.142 | | 16.98 | |
| 12.191 | | 17.05 | |

Distribution of plateau current $I_p$ for $e_w = 0.265$ was shown in Tab. 4.

Distribution of absolute uncertainties of plateau current $\Delta I_p$ for $e_w = 0.265$ are shown in Tab. 5.

Table 4: Distribution of plateau current $I_p \cdot 10^3$ [A] for $e_w = 0.265$.

| Re | Cathode No. | | | | | | |
|---|---|---|---|---|---|---|---|
| | 1 | 2 | 3 | 4 | 5 | 6 | 7 |
| 7700 | 8.508 | 10.6 | 11.18 | 12.11 | 11.1 | 10.71 | 11.47 |
| 9700 | 9.66 | 12.5 | 13.21 | 13.86 | 13.3 | 12.65 | 13.07 |
| 11700 | 11.36 | 13.84 | 14.27 | 15.42 | 15.08 | 14.25 | 14.64 |
| 13600 | 12.03 | 15.51 | 15.73 | 17.11 | 16.94 | 16.01 | 16.04 |
| 16600 | 13.03 | 17.41 | 17.88 | 19.93 | 18.58 | 17.35 | 17.71 |
| 20500 | 14.3 | 18.97 | 20.33 | 21.12 | 20.51 | 18.77 | 19.5 |
| 24500 | 16.2 | 20.69 | 21.22 | 23.64 | 22.64 | 20.57 | 21.94 |
| 29400 | 18.9 | 23.68 | 23.26 | 25.25 | 25.33 | 23.0 | 24.13 |
| 35300 | 20.32 | 25.69 | 26.22 | 29.53 | 28.78 | 26.13 | 26.71 |

Table 5: Distribution of absolute plateau current uncertainties $\Delta I_p \cdot 10^5$ [A] for $e_w = 0.265$.

| Re | Cathode No. | | | | | | |
|---|---|---|---|---|---|---|---|
| | 1 | 2 | 3 | 4 | 5 | 6 | 7 |
| 7700 | 3.46 | 4.04 | 4.28 | 4.65 | 4.24 | 4.08 | 4.35 |
| 9700 | 3.93 | 4.77 | 5.06 | 5.32 | 5.08 | 4.82 | 4.96 |
| 11700 | 4.62 | 5.28 | 5.46 | 5.92 | 5.76 | 5.43 | 5.56 |
| 13600 | 4.89 | 5.92 | 6.02 | 6.56 | 6.47 | 6.10 | 6.22 |
| 16600 | 5.41 | 6.64 | 6.84 | 7.65 | 7.10 | 6.61 | 6.72 |
| 20500 | 5.82 | 7.23 | 7.78 | 8.10 | 7.83 | 7.15 | 7.40 |
| 24500 | 6.59 | 7.89 | 8.12 | 9.07 | 8.65 | 7.84 | 8.33 |
| 29400 | 7.69 | 9.03 | 8.90 | 9.69 | 9.67 | 8.76 | 9.16 |
| 35300 | 8.27 | 9.80 | 10.03 | 11.33 | 10.99 | 9.96 | 9.14 |

On the basis of Eq. (2) the distribution of $h_D$ for $e_w = 0.265$ and $e_w = 0.0$ were shown in Tabs. 6 and 7, respectively.

Based on Eq. (2) and Tabs. 2–4, and 8 the absolute uncertainty of the mass transfer coefficient measurement was given by

$$\Delta h_D = \sqrt{\left(\frac{\partial h_D}{\partial I_p}\Delta I_p\right)^2 + \left(\frac{\partial h_D}{\partial A_K}\Delta A_K\right)^2 + \left(\frac{\partial h_D}{\partial C_p}\Delta C_p\right)^2} \qquad (12)$$

Table 6: Distribution of $h_D \cdot 10^5$ [m/s] for $e_w = 0.265$.

| Re | Cathode No. | | | | | | |
|---|---|---|---|---|---|---|---|
| | 1 | 2 | 3 | 4 | 5 | 6 | 7 |
| 7700 | 3.46 | 4.04 | 4.28 | 4.65 | 4.24 | 4.08 | 4.35 |
| 9700 | 3.93 | 4.77 | 5.06 | 5.32 | 5.08 | 4.82 | 4.96 |
| 11700 | 4.62 | 5.28 | 5.46 | 5.92 | 5.76 | 5.43 | 5.56 |
| 13600 | 4.89 | 5.92 | 6.02 | 6.56 | 6.47 | 6.10 | 6.22 |
| 16600 | 5.41 | 6.64 | 6.84 | 7.65 | 7.10 | 6.61 | 6.72 |
| 20500 | 5.82 | 7.23 | 7.78 | 8.10 | 7.93 | 7.15 | 7.40 |
| 24500 | 6.59 | 7.89 | 8.12 | 9.07 | 8.65 | 7.84 | 8.33 |
| 29400 | 7.69 | 9.03 | 8.90 | 9.69 | 9.67 | 8.76 | 9.16 |
| 35300 | 8.27 | 9.80 | 10.03 | 11.33 | 10.99 | 9.96 | 10.14 |

Table 7: Distribution of $h_D \cdot 10^5$ [m/s] for $e_w = 0.0$.

| Re | Cathode No. | | | | | | |
|---|---|---|---|---|---|---|---|
| | 1 | 2 | 3 | 4 | 5 | 6 | 7 |
| 7700 | 3.46 | 4.04 | 4.28 | 4.65 | 4.24 | 4.08 | 4.35 |
| 9700 | 3.93 | 4.77 | 5.06 | 5.32 | 5.08 | 4.82 | 4.96 |
| 11700 | 4.62 | 5.28 | 5.46 | 5.92 | 5.76 | 5.43 | 5.56 |
| 13600 | 4.89 | 5.92 | 6.02 | 6.56 | 6.47 | 6.10 | 6.22 |
| 16600 | 5.41 | 6.64 | 6.84 | 7.65 | 7.10 | 6.61 | 6.72 |
| 20500 | 5.82 | 7.23 | 7.78 | 8.10 | 7.93 | 7.15 | 7.40 |
| 24500 | 6.59 | 7.89 | 8.12 | 9.07 | 8.65 | 7.84 | 8.33 |
| 29400 | 7.69 | 9.03 | 8.90 | 9.69 | 9.67 | 8.76 | 9.16 |
| 35300 | 8.27 | 9.80 | 10.03 | 11.33 | 10.99 | 9.96 | 10.14 |

and shown in Tab. 9, where the bulk concentration of potassium hexacyanoferrate (III) ions $C_b$ and its uncertainty $\Delta C_b$ for $e_w = 0.0$ and 0.265 were shown in Tab. 8.

Table 8: Bulk concentration of potassium hexacyanoferrate (III) ions.

| $e_w$ | $C_b \cdot 10^3$ kmol/m$^3$ | $\Delta C_b \cdot 10^5$ kmol/m$^3$ |
|---|---|---|
| 0.0 | 3.52 | 8.48 |
| 0.265 | 2.24 | 8.71 |

Table 9: Mean value of mass transfer coefficient $h_{Dm}$ and its absolute uncertainty for $e_w = 0.265$ and $e_w = 0.0$, respectively.

| Re | 7700 | 9700 | 11700 | 13600 | 16600 | 20500 | 24500 | 29400 | 35300 |
|---|---|---|---|---|---|---|---|---|---|
| $h_{D_{0.265}} \cdot 10^5$ [m/s] | 4.16 | 4.85 | 5.43 | 6.03 | 6.71 | 7.33 | 8.07 | 8.99 | 10.1 |
| $h_{D_{0.0}} \cdot 10^5$ [m/s] | 2.61 | 2.95 | 3.38 | 3.74 | 4.13 | 4.64 | 5.16 | 5.65 | 6.26 |
| $h_{D_{0.265}} \cdot 10^6$ [m/s] | 3.62 | 4.01 | 4.42 | 4.59 | 4.63 | 4.74 | 5.25 | 5.52 | 5.92 |
| $\Delta h_{D_{0.0}} \cdot 10^6$ [m/s] | 2.45 | 2.59 | 2.73 | 2.81 | 2.88 | 3.44 | 2.96 | 2.93 | 2.98 |
| $h_{D_{0.265}}$ [%] | 8.7 | 8.3 | 8.1 | 7.6 | 7,0 | 6.5 | 6.5 | 6.1 | 5.9 |
| $h_{D_{0.0}}$ [%] | 9.4 | 8.8 | 8.1 | 7.5 | 7,0 | 7.4 | 5.7 | 5.2 | 4.8 |

On the base of Eq. (8) the mean value of Sherwood number $\mathrm{Sh}_m$ vs Re for $e_w = 0.265$ and $e_w = 0.0$ as well as its absolute uncertainty were shown in Tab. 10, where $\Delta\mathrm{Sh}_{0.265}$ and $\Delta\mathrm{Sh}_{0.0}$ were calculated according to formula

$$\Delta\mathrm{Sh} = \sqrt{\left(\frac{\partial\mathrm{Sh}}{\partial h_D}\Delta h_D\right)^2 + \left(\frac{\partial\mathrm{Sh}}{\partial d_h}\Delta d_h\right)^2 + \left(\frac{\partial\mathrm{Sh}}{\partial D}\Delta D\right)^2}, \tag{13}$$

where $\Delta D = 2.35 \cdot 10^{-11}$ m$^2$/s [6].

Table 10: Mean value of Sherwood number Sh vs Re with its uncertainty for $e_w = 0.265$ and $e_w = 0.0$.

| Re | 7700 | 9700 | 11700 | 13600 | 16600 | 20500 | 24500 | 29400 | 35300 |
|---|---|---|---|---|---|---|---|---|---|
| $\mathrm{Sh}_{0.265}$ | 1050 | 1224 | 1371 | 1521 | 1694 | 1849 | 2037 | 2269 | 2543 |
| $\mathrm{Sh}_{0,0}$ | 658 | 745 | 852 | 944 | 1042 | 1172 | 1303 | 1426 | 1581 |
| $\Delta\mathrm{Sh}_{0.265}$ | 99 | 110 | 121 | 128 | 131 | 136 | 151 | 160 | 174 |
| $\Delta\mathrm{Sh}_{0.0}$ | 66 | 70 | 75 | 78 | 81 | 96 | 87 | 89 | 93 |
| $\mathrm{Sh}_{0.265}$ [%] | 9.4 | 9.0 | 8.8 | 8.4 | 7.7 | 7.3 | 7.4 | 7.1 | 6.8 |
| $\mathrm{Sh}_{0.0}$ [%] | 10 | 9.4 | 8.8 | 8.3 | 7.8 | 8.2 | 6.7 | 6.2 | 5.9 |

Friction factor $f$ for $e_w = 0.265$ and $e_w = 0.0$ was calculated from Eq. (9) on the base of Tab. 11 and its absolute uncertainty was taken from

$$\Delta f = \sqrt{\left(\frac{\partial f}{\partial \Delta p}\delta\Delta p\right)^2 + \left(\frac{\partial f}{\partial \rho}\delta\rho\right)^2 + \left(\frac{\partial f}{\partial w}\delta w\right)^2 + \left(\frac{\partial f}{\partial L_o}\delta L_o\right)^2 + \left(\frac{\partial f}{\partial d_h}\delta d_h\right)^2}, \tag{14}$$

where $\delta\rho = 5.2$ kg/m$^3$ [5], $\delta\Delta p = 55$ Pa, 11 Pa for $e_w = 0.265$ and $e_w = 0.0$, respectively.

Table 11: Pressure drop and flow velocity in the duct for $e_w = 0.265$ and $e_w = 0.0$.

| Re | 7700 | 9700 | 11700 | 13600 | 16600 | 20500 | 24500 | 29400 | 35300 |
|---|---|---|---|---|---|---|---|---|---|
| $\Delta p_{0.0}$ [kPa] | 0.05 | 0.14 | 0.27 | 0.5 | 0.78 | 1.2 | 1.73 | 2.63 | 3.98 |
| $\Delta p_{0.265}$ [kPa] | 0.59 | 1 | 1.58 | 2.24 | 3.27 | 4.51 | 6.14 | 8.84 | 13.04 |
| $w$ [m/s] | 0.48 | 0.6 | 0.72 | 0.84 | 1.02 | 1.26 | 1.5 | 1.8 | 2.16 |

Table 12: Friction factor and its absolute uncertainty vs Re for $e_w = 0.265$ and $e_w = 0.0$.

| Re | 7700 | 9700 | 11700 | 13600 | 16600 | 20500 | 24500 | 29400 | 35300 |
|---|---|---|---|---|---|---|---|---|---|
| $f_{0.0}$ | 0.05 | 0.09 | 0.12 | 0.16 | 0.17 | 0.17 | 0.18 | 0.19 | 0.20 |
| $f_{0.265}$ | 0.59 | 0.64 | 0.70 | 0.73 | 0.72 | 0.65 | 0.63 | 0.63 | 0.64 |
| $\Delta f_0$ | 0.0166 | 0.0192 | 0.0205 | 0.0239 | 0.0207 | 0.0172 | 0.0147 | 0.0133 | 0.0118 |
| $\Delta f_{0.265}$ | 0.147 | 0.128 | 0.117 | 0.106 | 0.086 | 0.064 | 0.052 | 0.045 | 0.039 |
| $\Delta f_0\%$ | 25 | 20 | 17 | 15 | 12 | 10 | 8 | 7 | 6 |
| $\Delta f_{0.265}\%$ | 33 | 21 | 17 | 15 | 12 | 10 | 8 | 7 | 6 |

Friction factor and its uncertainty vs Re for $e_w = 0.265$ and $e_w = 0.0$ was shown in Tab. 12.

On the basis of Fig. 10 and Eq. (7) $Q = Q_{\max}$ was given by

$$Q_{\max} = \frac{\mathrm{Sh}_{0.265} - \mathrm{Sh}_{0.0}}{f_{0.265} - f_{0.0}} \tag{15}$$

and on the basis of Tab. 12 its absolute and relative uncertainty was calculated from

$$\Delta Q_{\max} = $$

$$= \sqrt{\left(\frac{\partial Q_{\max}}{\partial \mathrm{Sh}_{0.265}}\delta \mathrm{Sh}_{0.265}\right)^2 + \left(\frac{\partial Q_{\max}}{\partial \mathrm{Sh}_{0.0}}\delta \mathrm{Sh}_{0.0}\right)^2 + \left(\frac{\partial Q_{\max}}{\partial f_{0.265}}\delta f_{0.265}\right)^2 + \left(\frac{\partial Q_{\max}}{\partial f_{0.0}}\delta f_{0.0}\right)^2} \tag{16}$$

and

$$\Delta Q_{\max}\ [\%] = \frac{\Delta Q_{\max}}{Q_{\max}} \times 100\,. \tag{17}$$

Finally, $Q_{\max}$ and its uncertainty was shown in Tab. 13.

Table 13: Distribution of $Q_{\max}$ and its uncertainty.

| Re | 7700 | 9700 | 11700 | 13600 | 16600 | 20500 | 24500 | 29400 | 35300 |
|---|---|---|---|---|---|---|---|---|---|
| $Q_{\max}$ | 727 | 874 | 895 | 1021 | 1187 | 1415 | 1632 | 1916 | 2158 |
| $\Delta Q_{\max}$ | 221 | 239 | 247 | 265 | 281 | 348 | 387 | 418 | 443 |
| $\Delta Q_{\max}$ [%] | 30 | 27 | 28 | 26 | 24 | 25 | 24 | 22 | 21 |

Table 14: Values of Sh and $f$ absolute uncertainties.

| $\Delta$ Sh | | | | | | | | | |
|---|---|---|---|---|---|---|---|---|---|
| $e_w$ | Re | | | | | | | | |
| | 7700 | 9700 | 11700 | 13600 | 16600 | 20500 | 24500 | 29400 | 35300 |
| 0.0 | 66 | 70 | 75 | 78 | 81 | 96 | 88 | 89 | 93 |
| 0.089 | 63 | 66 | 69 | 82 | 73 | 79 | 83 | 92 | 93 |
| 0.177 | 52 | 56 | 63 | 64 | 71 | 77 | 77 | 82 | 86 |
| 0.265 | 99 | 110 | 121 | 128 | 131 | 136 | 151 | 160 | 174 |
| 0.354 | 135 | 150 | 169 | 169 | 188 | 203 | 211 | 231 | 252 |
| $\Delta f$ | | | | | | | | | |
| $e_w$ | Re | | | | | | | | |
| | 7700 | 9700 | 11700 | 13600 | 16600 | 20500 | 24500 | 29400 | 35300 |
| 0.0 | 0.017 | 0.019 | 0.021 | 0.024 | 0.021 | 0.017 | 0.015 | 0.013 | 0.012 |
| 0.089 | 0.071 | 0.058 | 0.048 | 0.045 | 0.033 | 0.025 | 0.020 | 0.017 | 0.015 |
| 0.177 | 0.120 | 0.092 | 0.076 | 0.066 | 0.050 | 0.038 | 0.031 | 0.026 | 0.023 |
| 0.265 | 0.147 | 0.128 | 0.117 | 0.106 | 0.086 | 0.064 | 0.052 | 0.045 | 0.039 |
| 0.354 | 0.331 | 0.300 | 0.271 | 0.243 | 0.189 | 0.145 | 0.116 | 0.102 | 0.100 |

On the basis of Eq. (10), Tab. 2 and Tab. 14 the absolute and relative uncertainty of $E$ function were calculated respectively:

$$\Delta E_i = \sqrt{\left(\frac{\partial E}{\partial \mathrm{Sh}_i}\delta \mathrm{Sh}_i\right)^2 + \left(\frac{\partial E}{\partial \mathrm{Sh}_0}\delta \mathrm{Sh}_0\right)^2 + \left(\frac{\partial E}{\partial f_i}\delta f_i\right)^2 + \left(\frac{\partial E}{\partial f_0}\delta f_0\right)^2} \tag{18}$$

and

$$\delta \Delta E_i\% = \frac{E_i}{E_i}100 \tag{19}$$

and their distributions were given in Tabs. 15 and 16.

Table 15: Distribution of absolute uncertainties $\Delta E$.

| $e_w$ | Re | | | | | | | | |
|---|---|---|---|---|---|---|---|---|---|
| | 7700 | 9700 | 11700 | 13600 | 16600 | 20500 | 24500 | 29400 | 35300 |
| 0.089 | 0.085 | 0.091 | 0.100 | 0.098 | 0.112 | 0.136 | 0.149 | 0.165 | 0.174 |
| 0.178 | 0.056 | 0.063 | 0.068 | 0.072 | 0.083 | 0.099 | 0.109 | 0.119 | 0.127 |
| 0.265 | 0.058 | 0.058 | 0.057 | 0.059 | 0.064 | 0.076 | 0.086 | 0.095 | 0.104 |
| 0.354 | 0.032 | 0.032 | 0.032 | 0.034 | 0.038 | 0.045 | 0.051 | 0.055 | 0.053 |

Table 16: Distribution of relative uncertainties $\delta E$ %.

| $e_w$ | Re | | | | | | | | |
|---|---|---|---|---|---|---|---|---|---|
| | 7700 | 9700 | 11700 | 13600 | 16600 | 20500 | 24500 | 29400 | 35300 |
| 0.089 | 43 | 25 | 20 | 16 | 16 | 18 | 19 | 20 | 21 |
| 0.178 | 42 | 25 | 20 | 16 | 16 | 18 | 19 | 20 | 21 |
| 0.265 | 43 | 25 | 21 | 16 | 17 | 18 | 20 | 20 | 21 |
| 0.354 | 43 | 25 | 21 | 16 | 17 | 18 | 20 | 20 | 21 |

# 6 Conclusions

Increasing of the efficiency of convective cooling of the inner surface of a short duct by changing its geometry was studied by the use of the electrochemical limiting current technique.

A the chosen geometry of the studied duct and by the use of $Q$ function the most profitable conditions of heat/ mass transfer were determined. The $Q$ function describes the change of heat/mass transfer related to the change of flow resistance. The changes were related to the smooth duct (Figs. 8 and 9). $Q = Q_{\max}$ (Fig. 10, Tab. 1) determines the displacement ($e_w = 0.265$) at which the ratio $\Delta\mathrm{Sh}/\Delta f$ had the highest value. $Q_{\max}$ value was calculated with uncertainties of (21–30)% in the studied range of Reynolds number. As can be seen in Fig. 10 the conditions of heat/ mass transfer are the most profitable at the one displacement $e_w$ regardless of the studied range of Reynolds number (7700–35300).

The duct efficiency has been described by the function $E = (\mathrm{Sh}/f)/(\mathrm{Sh}_0/f_0)$. As can be seen in Fig. 11 the duct efficiency decreases with the increase of $e_w$ displacement. However at $e_w = 0.265$ intensity of the efficiency drop is decreasing.

The heat/ mass transfer enhancement in presented geometrical configuration occurs partially as a result of vortex shedding process which increases turbulence intensity. The vortex shedding takes place on sharp edges of the test rings of the duct, just like on a bluff body [13, 14]. By using flow inserts like ribs, winglets or sharp edge, the flow can be more turbulent, which increases heat/mass transfer coefficient [15, 16]. The vortex shedding process occurs to be the most favorable at $e_w = 0.265$ displacement of the tested duct.

The tested duct could be used in design works on heat exchangers and channels for cooling of turbine blades or electronic equipment.

**Acknowledegment** The author would like to acknowledge the help of Professors Bogumił Bieniasz and Joanna Wilk in realization of the work.

*Received 1 April 2019*

## References

[1] Bieniasz B.: *Short ducts consisting of cylindrical segments and their convective mass/heat transfer, pressure drop and performance analysis*. Int. J. Heat Mass Tran. **41**(1998), 3, 501–511.

[2] Sethumadhavan R., Raja Rao M.: *Turbulent flow heat transfer and fluid friction in helical–wire–coil–inserted tubes*. Int. J. Heat Mass Tran. **26**(1983), 12, 1833–1845.

[3] Liao Q., Xin M.D.: *Augmentation of convective heat transfer inside tubes with three dimensional internal extended surfaces and twisted-tape inserts*. Chem. Eng. J. **78**(2000), 95–105.

[4] Chang S.W., Yang T.L., Huang C.C., Chiang K.F.: *Endwall heat transfer and pressure drop in rectangular channels with attached and detached circular pin-fin array*. Int. J. Heat Mass Tran. **51**(2008), 5247–5259.

[5] Welty J.R., Wicks C.E., Wilson R.E, Rorrer G.E.: *Fundamentals of Momentum, Heat, and Mass Transfer*. Willey, Hoboken 2008, ISBN-13 978-0470128688.

[6] Bieniasz B., Wilk J.: *Forced convection mass/heat transfer coefficient at the surface of the rotor of the sucking and forcing regenerative exchanger*. Int. J. Heat Mass Tran. **38**(1995), 10, 1823–1830.

[7] Wilk J.: *Mass/heat transfer coefficient in the radially rotating circular channels of the rotor of the high-speed heat regenerator*. Int. J. Heat Mass Tran. **47**(2004), 1979–1988.

[8] Lucas D.M., Davies R.M.: *Mass transfer modelling techniques in the prediction of convective heat transfer coefficients in industrial heating processes*. In: Proc. Fourth Int. Heat Transfer Conf., Paris, Versailles, vol. VII, Paper MT 1.2., Elsevier, Amsterdam, 1970.

[9] Wilk J.: *A review of measurements of the mass transfer in minichannels using the limiting current technique*. Exp. Therm. Fluid Sci. **57**(2014), 242–249.

[10] Wilk J.: *Convective mass/heat transfer in the entrance region of the short circular minichannel*. Exp. Therm. Fluid Sci. **38**(2012), 107–114

[11] Wilk J.: *Experimental investigations on convective mass/heat transfer in short minichannel at low Reynolds numbers*. Exp. Therm. Fluid Sci. **33**(2009), 267–272.

[12] Wilk J., Grosicki S., Kiedrzyński K.: *Preliminary research on mass/heat transfer in mini heat exchanger*. E3S Web of Conferences 70, 02016 (2018), https:/doi.org/10.1051/e3sconf/20187002016.

[13] Gil P.: *Bluff body drag control using synthetic jet*. J. Appl. Fluid Mech. **12**(2019), 1, 293–302.

[14] Strzelczyk P., Gil P.: *Properties of velocity field in the vicinity of synthetic jet generator*. In: Journal of Physics: Conf. Ser. **760**(2016), 1, p. 012029. IOP Publishing.

[15] Han J.C., Park J.S.: *Developing heat transfer in rectangular channels with rib turbulators*. Int. J. Heat Mass Tran. **31**(1988), 1, 183–195.

[16] Ali M.M., Ramadhyani S.: *Experiments on convective heat transfer in corrugated channels*. Int. J. Heat Mass Tran. **5**(1992), 3, 175–193.

[17] Andrzejczyk R., Muszyński T.: *Thermal and economic investigation of straight and U-bend double tube heat exchanger with coiled wire turbulator*. Arch. Thermodyn. **40**(2019), 2, 17–33.